Nonlinear evolution of the Weibel instability of relativistic electron beams

Article *in* Physics of Plasmas · March 2009

DOI: 10.1063/1.3093477

CITATIONS
18

READS
58

5 authors, including:

Gennady Shvets
University of Texas at Austin
410 PUBLICATIONS **8,517** CITATIONS

SEE PROFILE

Igor Kaganovich
Princeton University
321 PUBLICATIONS **2,587** CITATIONS

SEE PROFILE

Nonlinear evolution of the Weibel instability of relativistic electron beams[a)]

Gennady Shvets,[1,b)] Oleg Polomarov,[2] Vladimir Khudik,[1] Carl Siemon,[1] and Igor Kaganovich[3]
[1]*Department of Physics and Institute for Fusion Studies, The University of Texas at Austin, Austin, Texas 78712, USA*
[2]*Fusion Science Center, Laboratory for Laser Energetics, University of Rochester, New York 14623, USA*
[3]*Plasma Physics Laboratory, Princeton University, Princeton, New Jersey 08543, USA*

(Received 12 December 2008; accepted 11 February 2009; published online 24 March 2009)

Physics of the long-term evolution of the Weibel instability (WI) of an electron beam propagating through the plasma is described. Several phenomena occurring during the WI are identified: (i) the exponential growth stage resulting in beam breakup into small current filaments; (ii) merger of the small filaments and beam particles' trapping inside them; (iii) filaments' compression and expulsion of the ambient plasma from the filaments; (iv) formation of high-current filaments and their merger. It is shown that during the final stage these beam filaments can carry super-Alfvenic currents and form hollow current density profiles similar to the Hammer–Rostoker equilibrium. This explains why the initially increasing magnetic field energy eventually decreases during the late stage of the instability. Different computational approaches to modeling both collisionless and collisional WI are also described. © *2009 American Institute of Physics*. [DOI: 10.1063/1.3093477]

I. INTRODUCTION AND EARLIER WORK

The Weibel instability[1–5] (WI) of plasmas with anisotropic velocity distribution is one of the most basic and long-studied collective plasma processes. For example, propagation of an electron beam through the background plasma is subject to strong WI.[2] There has been a significant revival in theoretical studies of the WI because it is viewed as highly relevant to at least two areas of science: astrophysics of gamma-ray bursts and their afterglows[6–11] and the fast ignitor[12] scenario of the inertial confinement fusion. Specifically, generation of the upstream magnetic field during the gamma-ray bursts' (GRB) aftershocks is considered necessary for explaining emission spectra of the afterglows as well as for generating and sustaining collisionless shocks responsible for particle acceleration during GRBs. Collisionless WI is the likeliest mechanism[6–11] for producing such magnetic fields. The WI is likely to play an important role in the fast ignitor scenario[12] because it can result in the collective energy loss of a relativistic electron beam in both coronal and core plasma regions.[12–20] Because the relativistic electron beam has to travel through an enormous density gradient (density variation from 10^{22} cm^{-3} near the critical surface where the beam is produced to 10^{26} cm^{-3} in the dense core where the ignition occurs), both collisionless and collisional WI manifest themselves along the beam's path.

The dynamics and energetics of the nonlinear saturation and long-term behavior of the WI are important for both laboratory and astrophysical plasmas. For example, collisionless shock dynamics depends on the long-term evolution of the magnetic field energy. Specifically, it is not clear whether the long-term magnetic fields generated during the coalescence of current filaments remain finite[16] or decay with time[8] (and if they do, according to what physical mechanism). Numerous numerical simulations[3,21] demonstrated that the magnetic field energy grows during the earlier stages of the WI and starts decaying during the later (strongly nonlinear) stage. The reason for this decay has never been fully understood. One decay mechanism, based on the merger of filaments bearing super-Alfvenic current ($I > I_A = \gamma\beta mc^3/e$,[22] where $-e$ and m are the electron charge and mass, respectively, and c is the speed of light in vacuum) during the late stage of the WI, has been recently identified.[23] In this review we present a detailed analysis of the high-current filaments' current and density profiles and provide qualitative and quantitative explanation of the energetics of their merger. We demonstrate that the final nonlinear stage of the WI is characterized by the energy transfer from the magnetic field to plasma particles, making it reminiscent of magnetic reconnection.

Additionally, we review several computational techniques for modeling WI: (a) direct fully electromagnetic particle-in-cell (PIC) simulations that model both beam and ambient plasma's particles using computational macroparticles, (b) quasineutral (QN) simulations that assume charge neutrality of the system consisting of the beam electrons, ambient plasma electrons, and ambient plasma ions,[19] and (c) quasiequilibrium (QE) simulations that assume force equilibrium of the ambient electron plasma without assuming charge neutrality. Both QN and QE simulations do not resolve the motion of the ambient plasma electrons and, therefore, can take computational time steps $\Delta t > 1/\omega_{p0}$, where $\omega_{p0} = \sqrt{4\pi e^2 n_0/m}$ is the electron plasma frequency, and n_0 is the uniform ion density. Because the initial growth rate of the WI given by

$$\Gamma_{\mathrm{WI}} = \frac{\beta_{b0}\omega_{p0}}{\sqrt{\gamma_{b0}}}\sqrt{\frac{n_{b0}}{n_{p0}}} \tag{1}$$

(where n_{b0} and γ_{b0} are the initial beam density and relativistic factor, respectively) can be much smaller than ω_{p0},

[a)]Paper GI2 4, Bull. Am. Phys. Soc. **53**, 82 (2008).
[b)]Invited speaker.

larger time step means considerable reduction in the computational time. This is especially important for fast ignition problems, where the beam must propagate through very dense plasmas with $n_{p0} \gg n_{b0}$, and the beam's relativistic factor $\gamma_{b0} \gg 1$.

In this review we concentrate on the physics and computational modeling of a two-dimensional (2D) WI, i.e., we use a simplified model which is 2D in space (very long electron beam propagating in the homogeneous z-direction) and three-dimensional (3D) in the plasma and beam momenta. By neglecting the z-variation, collective instabilities such as the electrostatic two stream are neglected. The two-stream instability (TSI) has been shown[24–26] to saturate by beam electron trapping before extracting a relatively small fraction of the beam energy. Additional factors that make the TSI less important than the WI are γ_b^{-1} scaling[27] of its growth rate for relativistic beams, its resonant nature ($\omega_{\mathrm{TSI}} \approx \omega_{p0}$) that makes it susceptible to both transverse and longitudinal density gradients, and finite plasma temperature and its return streaming velocity can also suppress the TSI. The full 3D interplay between WI and TSI is beyond the scope of this review, and will be addressed elsewhere. With the exception of Sec. IV, plasma ions are assumed to be infinitely heavy, forming a charge-neutralizing stationary background of density n_0.

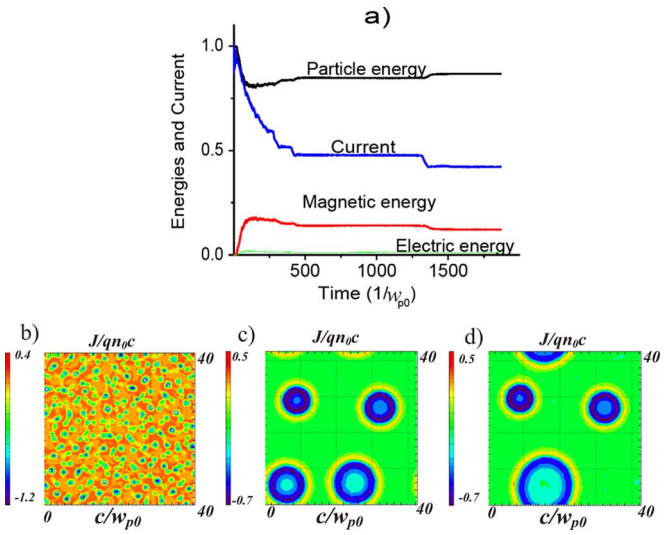

FIG. 1. (Color online) Full PIC simulations of the WI of a relativistic beam in plasma using LSP. (a) Long-term evolution of the magnetic and electric field energies, plasma energy, and normalized beam current. Energies are normalized to the initial total energies of the beam and plasma. Bottom panel: current density for $\omega_{p0}t=50$ (b), $\omega_{p0}t=1300$ (c), and $\omega_{p0}t=1600$ (d). Beam parameters: $n_{b0}/n_0=0.2$ and $\beta_{b0}=0.95$. Beam initially fills the simulated $40c/\omega_{p0} \times 40c/\omega_{p0}$ computational domain. "Steps" in the energy and current plots correspond to the merger of large filaments (see text for details).

II. DESCRIPTION OF NUMERICAL TOOLS FOR MODELING THE WEIBEL INSTABILITY

A. Full particle-in-cell codes: Examples

Conventional PIC codes have been used to model the WI for almost 30 years.[3–5,15,16,20,23] Explicit electromagnetic PIC codes advance electric and magnetic fields in time according to the full set of Maxwell's equations, and use either macroparticle description of the beam and plasma particles, or a simplified fluid description[15] of the ambient plasma. In either case, the time step Δt must satisfy $\Delta t < \omega_{p0}^{-1}$. This condition can be relaxed in the codes that utilize an implicit particle push.[28]

We use the results of such simulation to illustrate different stages of the nonlinear WI whose detailed physics is addressed in Sec. III. We have used the LSP PIC code[29] to simulate the WI of a spatially uniform cold electron beam with $n_{b0}/n_0=0.2$ and $\beta_{b0}=0.95$. Initially, the beam is assumed to be charge and current neutralized by the ambient plasma. Periodic conditions are applied at the boundaries of the square $L \times L$ (where $L=40c/\omega_{p0}$) domain. The total initial beam current is $I_{0b} \approx 8I_A$. Simulation results are presented in Fig. 1, where the magnetic field energy normalized to the initial beam energy $\gamma_{b0}n_{b0}mc^2L^2$ (both per unit length in z) is plotted in Fig. 1(a), and a sequence of current density snapshots taken at different times is shown in Figs. 1(b)–1(d). By inspecting the time evolution of the magnetic field, we identify the following stages of the WI instability.

The earliest stage results in filaments' formation and exponential growth of the magnetic field with the temporal growth rate Γ_{WI}. The typical size of a filament is of order $\delta \approx c/\omega_{p0}$. Filaments' formation manifests itself in beam density increase δn_b inside the filaments[19] which also grows exponentially. This exponential growth saturates due to magnetic trapping of the beam particles[3,4] when $\delta n_b \sim n_{b0}$, or at around $t=25\omega_{p0}^{-1}$ in the present simulation. Magnetic trapping occurs when the bounce frequency Ω_b of a beam electron inside the current-carrying (uncompensated by the return current) beam filament becomes equal to the linear growth of the WI: $\Omega_b \sim \gamma_{\mathrm{WI}}$. This condition is satisfied when $\delta n_b \sim n_{b0}$. Magnetic trapping is further explained and illustrated in Sec. III A, where a simplified (QN) particle code is used for modeling the early stage of the WI.

Beam density inside the filaments (and, consequently, magnetic field energy) continues growing after the trapping limit is achieved, although at the reduced rate as numerically demonstrated in Sec. III A. As the filaments merge and grow, beam temperature and density inside them also grow until the filaments' beam density reaches the ambient plasma ion density n_0. At that point all electrons of the ambient plasma are expelled from the filament, although the filaments remain charge neutralized by the ions. Examples of small plasma-depleted filaments are shown in Fig. 1(b) for $t=50\omega_{p0}^{-1}$. The structure of plasma-depleted charge-neutralized beam filaments is considered in Sec. III B using a simplified analytic model. Further magnetic energy increase also occurs through the merger of the small magnetic filaments. Because the beam density inside the evacuated filament remains fixed at $n_b=n_0$, filaments' merger results in their enlargement. For example, if two current filaments of areas A_1 and A_2 merge to form a single filament of the area A_3, then, by conservation of beam particles, $A_3=A_1+A_2$.

As small filaments merge, their typical radius R_0 exceeds several collisionless skin depths. It can be shown that when $R_0 > c/\omega_{p0}$, the current per filament exceeds I_A. Whether filament currents can exceed I_A has been a subject of some debate, and it has been suggested in a number of

publications[5,10,30] that the per filament current produced via the WI is limited to I_A. Our simulations demonstrate that this is not the case, and that currents $I \gg I_A$ can be transported by electron plasma-void (EPV) beam filaments. Examples of current density profiles corresponding to multi-I_A filaments are shown in Figs. 1(c) and 1(d). Detailed particle and current density profiles for these filaments and their relation to the Hammer–Rostoker[31] equilibria are examined in Sec. III C. Although the existence of charged-neutralized self-pinched multi-I_A beams is well known,[22,31] this is the first identification of such current filaments self-consistently produced in the course of the WI. As it turns out, the presence of such filaments is crucial for explaining the most surprising aspect of the magnetic energy evolution: that the magnetic energy eventually stops growing and starts decaying as seen in Fig. 1(a). While this behavior has been previously observed in both 2D (Ref. 3) and 3D (Ref. 16) simulations, it has never been explained. We demonstrate that the magnetic energy decrease is related to the merger between multi-I_A filaments and energy transfer to the plasma particles. The resulting process is strongly reminiscent of the magnetic reconnection, where magnetic energy is transferred from magnetic field to particles. Note that large filaments' merger is clearly observed in Fig. 1(a): It corresponds to stepwise changes in the transported beam current and magnetic field energy.

Full PIC simulations indicate (see, for example, Fig. 5) that for $\gamma_b \gtrsim 1$ QN is accurately preserved during all stages of the WI instability: $n_p + n_b \approx n_0$. This observation leads us to consider a simplified alternative to full-PIC simulations: a QN code.

B. Quasineutral codes

The logic behind the QN code is that the full dynamics of the ambient plasma need not be simulated, and its density can be obtained from the QN condition,

$$n_{pe}(\vec{x}) = n_0 - n_b(\vec{x}). \tag{2}$$

Therefore, ambient plasma is modeled as a passive fluid that responds to the evolving electron beam by maintaining charge neutrality. In this section we assume that no EPV regions develop because Eq. (2) can only be applied as long as $n_{pe} > 0$. Violations of the QN condition are examined in Sec. II C.

Electron beam particles are modeled using numerical macroparticles that are advanced in time by the self-consistently determined electric and magnetic fields. The leading magnetic field $\vec{B}_\perp = -\vec{e}_z \times \vec{\nabla}_\perp \psi$ lies in the $x-y$ plane, where ψ is the z-component of the vector potential. The inductive electric field associated with the time-varying flux ψ is $E_z = -(1/c)\partial_t \psi$. Electric field also has a transverse component $\vec{E}_\perp$ that is found from the in-plane force balance of the ambient plasma electrons: $\vec{E}_\perp + \vec{v}_{pz} \times \vec{B}_\perp / c = 0$, where $\vec{v}_{pz} \equiv v_{pz}\vec{e}_z$ is the return flow of the ambient plasma. This QE is the consequence of another observation from direct PIC simulations: that the transverse velocity $\vec{v}_{p\perp}$ of the ambient plasma electrons is considerably smaller than the beam's average transverse speed $|\vec{v}_{b\perp}|$ and plasma's longitudinal velocity v_{pz}. One of the consequences of that is the magnetic field is predominantly transverse,[32] i.e., that the out-of-plane magnetic field is small: $|\vec{\nabla}\psi| \gg |B_z|$. To summarize, these are the dominant electric and magnetic fields of the QN beam-plasma system:

$$\vec{B}_\perp = -\vec{e}_z \times \vec{\nabla}_\perp \psi, \quad E_z = -\frac{1}{c}\frac{\partial \psi}{\partial t}, \quad \vec{E}_\perp = -(v_{pz}/c)\vec{\nabla}_\perp \psi. \tag{3}$$

Note[19] that for collisionless plasma the exact value of the electric field contains small inertial corrections proportional to the (small) $\vec{v}_{p\perp}$: $\vec{E}_\perp^{\text{exact}} = \vec{E}_\perp - (\delta\vec{E})_\perp$, where $(\delta\vec{E})_\perp = (m/e) \times [\partial_t \vec{v}_{p\perp} + \vec{\nabla}_\perp v_{p\perp}^2/2]$. Although $|(\delta\vec{E})_\perp| \ll |\vec{E}_\perp|$ for relativistic electron beams, this inertial correction is responsible[19] for generating an out-of-plane magnetic field B_z.

For collisionless plasma, two important conservation laws simplify the description of the plasma motion: conservation of the canonical momentum in the z-direction and the conservation of the generalized vorticity.[19,33,34] The former is essential for deriving the field equation for ψ that defines the dominant in-plane magnetic field. The latter can be used for computing the (less dynamically important) out-of-plane magnetic field B_z. Conservation of the canonical momentum translates into the nonrelativistic expression for the plasma return velocity: $v_{pz}/c = \tilde{\psi}$ (or $v_{pz}/c = \tilde{\psi}/\sqrt{1+\tilde{\psi}^2}$ in the relativistic case), where $\tilde{\psi} = e\psi/mc^2$ is the dimensionless vector potential. For resistive plasma, canonical momentum is no longer conserved, and the collisions frequency ν must be taken into account when calculating the plasma velocity: $\partial_t v_{pz} + \nu v_{pz} = (e/mc)\partial_t \psi$. From Ampere's law then follows that

$$\nabla_\perp^2 \psi - 4\pi e n v_{pz}/c = -4\pi J_{bz}/c, \tag{4}$$

where the displacement current is neglected to be consistent with the QN assumption. The z-component of the beam electron current is calculated from the beam's macroparticles' contribution: $J_{bz} = -\Sigma_j q_j v_{jz} \delta^2(\vec{x} - \vec{x}_j)/L_z$, where index j labels numerical macroparticles, and q_j/L_z and M_j/L_z are the macroparticle's charge and mass per unit length. For nonrelativistic collisionless plasma Eq. (4) is simplified to $\nabla_\perp^2 \psi - k_{pe}^2 \psi = -4\pi J_{bz}/c$, where the spatially nonuniform $k_{pe}^2 \equiv \omega_{pe}^2/c^2$ is obtained from Eq. (2) through $\omega_{pe}^2(\vec{x}) = 4\pi e^2 n_e(\vec{x})/m$. This equation is easily generalized to the case of relativistic electron plasma.

Conservation of the generalized vorticity $\vec{\Omega} \equiv \vec{\nabla} \times \vec{v}_p - e\vec{B}/mc$ (Refs. 33 and 34) enables us to derive[19] an equation for B_z using the conservation of Ω_z,

$$n_{pe}\vec{\nabla}_\perp \cdot \left(\frac{\vec{\nabla}_\perp B_z}{n_{pe}}\right) - \frac{\omega_{pe}^2}{c^2}B_z + \frac{4\pi n_{pe}}{c}\vec{e}_z \cdot \left(\vec{\nabla}_\perp \times \frac{\vec{J}_{b\perp}}{n_{pe}}\right) = 0, \tag{5}$$

where we have used the fact that for initially quiescent plasma, $\Omega_z = 0$ for all times. Note that despite the formal similarity between Eqs. (4) and (5), they predict very different magnitudes of $\vec{B}_\perp$ and B_z because the right hand side in

Eq. (4) is the longitudinal beam current (large) while the right hand side in Eq. (5) is proportional to the curl of the transverse beam current (small). Specifically, $\vec{\nabla}_\perp \times \vec{J}_{b\perp}$ is small during the linear stage (when $\vec{J}_{b\perp}$ is mostly curl-free) and during the late filamentation stage (when the filaments are quasistationary, and $\vec{J}_{b\perp}$ is small). In resistive plasma Ω_z is no longer conserved and deviates from zero: $\partial_t \Omega_z = (\vec{\nabla}_\perp v_{pz} \times \vec{\nabla}_\perp \psi) \cdot \vec{e}_z$. The physical meaning of this vorticity change is that in the presence of collisions, there is a time lag between v_{pz} and ψ. This results in the differential drag of the in-plane magnetic field lines out of the plane by the plasma return current. Denoting the left hand side of Eq. (5) as Q, we find that

$$\frac{\partial Q}{\partial t} = -\frac{\omega_{pe}^2}{c^2}(\vec{\nabla}_\perp v_{pz} \times \vec{\nabla}_\perp \psi) \cdot \vec{e}_z. \tag{6}$$

Without plasma resistivity $Q=0$ because $\vec{\nabla}_\perp v_{pz} \equiv \vec{\nabla}_\perp \psi$, and the out-of-plane magnetic field is produced only through breaking up the electron beam into current filaments with a nonvanishing $\vec{\nabla} \times \vec{J}_{b\perp}$. Finite resistivity produces a nonvanishing Q and, therefore, can produce a finite B_z by converting some of $\vec{B}_\perp$ into B_z.

As in the standard PIC, beam electrons are modeled kinetically using macroparticles with the effective per unit length charges and masses q_j and M_j satisfying $q_j/M_j = e/m$, where index j labels numerical macroparticles. The longitudinal momentum of a beam electron (assumed collisionless owing to its relativistic energy) is found from the conservation of the canonical momentum,

$$\gamma_j v_{jz} = \gamma_{j0} v_{jz0} + \frac{e}{mc}(\psi - \psi_{j0}), \tag{7}$$

where we assume that the initial field in the plasma vanishes: $\psi_{j0}=0$. The transverse equation of motion for the beam electrons is

$$\frac{d(\gamma_j \vec{v}_{j\perp})}{dt} = -\frac{e(v_{jz} - v_{pz})}{mc}\vec{\nabla}_\perp \psi, \tag{8}$$

where the second term in the right hand side of Eq. (8) is due to the extra pinching of the electron beam provided by the transverse ambipolar electric field $\vec{E}_\perp = -(v_{pz}/c)\vec{\nabla}_\perp \psi$ that develops in response to the $\vec{v} \times \vec{B}$ expulsion of the electron plasma fluid. Note that $\vec{E}_\perp$ *counters* the magnetic expulsion of the ambient plasma, yet *reinforces* the magnetic pinching of the beam. The above expression for $\vec{E}_\perp$ is only valid in the absence of the complete plasma expulsion from the beam filaments, and needs to be modified when such expulsion takes place. As discussed in Sec. II C, charged ion sheaths develop whenever complete expulsion takes place, and $\vec{E}_\perp$ needs to be evaluated using Poisson's equation in the plasma-void regions. The expression for the transverse electric field is especially simple when the plasma is collisionless: $\vec{E}_\perp = -(mc^2/e)\vec{\nabla}_\perp \gamma_{p\|}$, where $\gamma_{p\|} = \sqrt{1+\tilde{\psi}^2}$.

To verify the validity of the QN approach, we have modeled the WI instability of a small low-density electron beam and compared the results with the full-PIC simulations using LSP.[19] A flattop cold cylindrical electron beam with the initial $\beta_{b0}=0.885c$, radius $10c/\omega_{p0}$, and $n_{b0}/n_{p0}=0.001$ was chosen to avoid plasma expulsion which would invalidate the QN approach. Snapshots of the beam density obtained using the QN and LSP codes are shown in Fig. 2. The agreement is very good given that different initial noise levels are present in the two codes. By taking larger time steps than $1/\omega_{p0}$ and by not simulating ambient plasma, the QN code provides a 30-fold run time speed-up compared to the LSP code. Note that this particular LSP run treated the background plasma particles as a fluid, whereas the electron beam particles were treated kinetically.

C. Quasiequilibrium codes

QN codes described in Sec. II B lose validity as soon as $n_b(\vec{x}) > n_0$ anywhere inside the simulation domain. Physically, this inequality corresponds to the full expulsion of the ambient electron plasma from a finite region in space, leading to the formation of the EPV regions. Outside of the EPV regions, $\vec{E}_\perp$ can still be computed from Eq. (3) owing to the QE of the electron plasma. This expression is no longer valid inside the EPV regions. In fact, the QN assumption expressed by Eq. (2) is no longer correct inside and near the EPV regions. Therefore, the electric field and the electron plasma density must be computed from Poisson's equation: $\vec{\nabla}_\perp \cdot \vec{E}_\perp = 4\pi e(n_0 - n_b - n_e)$, where n_b is obtained directly from the electron beam distribution numerically modeled by kinetic macroparticles.

For collisionless plasma, the electric field $\vec{E}_\perp \equiv -\vec{\nabla}_\perp \Phi$ is computed by solving Poisson's equation with the Dirichle boundary conditions at the EPV boundary: $-\nabla_\perp^2 \Phi = 4\pi e [n_0 - n_b(\vec{x})]$ *inside* the EPV regions (where $n_{pe}=0$), and $\Phi = (mc^2/e)\gamma_{p\|}$ *outside* of the EPV regions (where $n_{pe}>0$ and the QE condition is applicable). The corresponding electron density outside of the EPV regions is

$$n_{pe} = n_0 - n_b + n_0 c^2/\omega_{p0}^2 \nabla_\perp^2 \gamma_{p\|}. \tag{9}$$

Both Φ and its normal derivative must be continuous across the EPV boundary. Iteratively solving Poisson's equation for Φ in conjunction with Eq. (4) for ψ yields the electric and magnetic fields required for advancing the beam particles. Note that Φ is needed to establish the boundaries of the EPV regions while ψ is needed to set up boundary conditions for Φ at the EPV boundaries. Essentially, the electric potential Φ and the magnetic potential ψ are coupled to each other through the EPV boundaries which are self-consistently determined.

We note that the QN condition is violated only when electrons of the ambient plasma are relativistic. For example, when plasma electrons move near EPV region of cylindrical shape with the velocity close to c, the electric attraction should balance the magnetic expulsion of the plasma electrons so that the EPV region should have extra positive charge per unit length approximated by $\Delta Q = J_{bz}/c$.

An example of the QE simulation is shown in Fig. 3, where plasma response to three constant-density electron beams of variable shape and density n_b is computed within

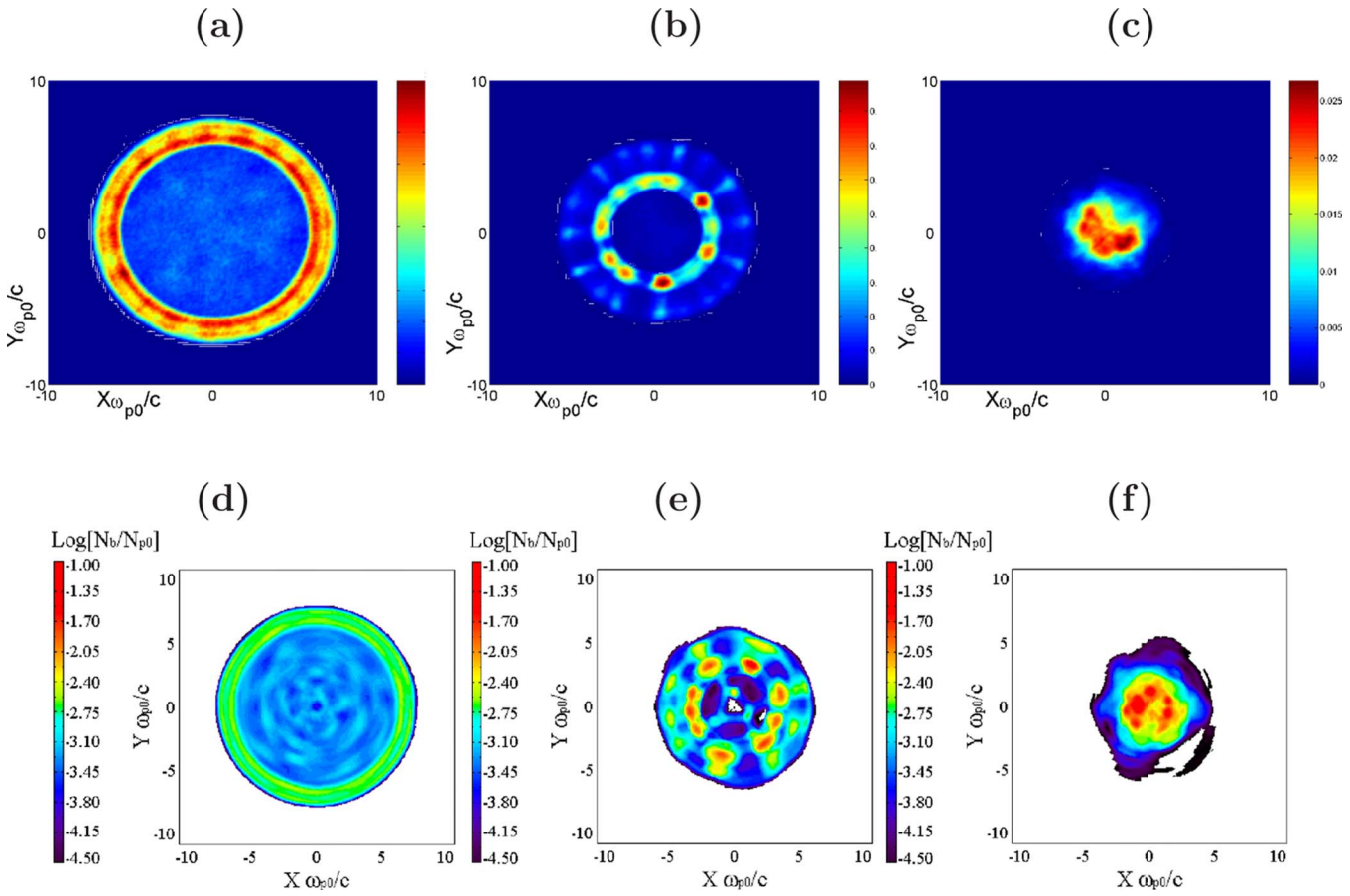

FIG. 2. (Color online) Comparison between QN and full-PIC simulations of the beam filamentation. Color map: electron beam density normalized to the ion density simulated by the QN code (top panel) and the full-PIC LSP code (bottom panel) for the following time snapshots: $\omega_{p0}t=220$; 380; 490 (from Ref. 19).

the QE framework. Several features are noteworthy. First, the QE approach correctly models EPV regions of an arbitrary shape. The outer regions (outside of the electron beam) of the EPV corresponding to the ion sheath (no electrons of any kind) with $\delta N \equiv (n_0 - n_e - n_b)/n_0 = 1$ are clearly visible. Second, electron plasma density $n_e > n_0$ immediately outside of the ion sheath ($\delta N < 0$) as required for overall charge neutrality. Finally, plasma response to sharp beam density profiles (e.g., square beam) can be accurately calculated. Note that the presented simulation is not fully self-consistent because the electron beam density and velocity are prescribed, i.e., beam electrons are not self-consistently evolved. Development of the self-consistent QE simulations will be reported elsewhere.

III. STAGES OF THE WEIBEL INSTABILITY

In Sec. I we have briefly outlined several evolution stages of the WI. Below the physical phenomena occurring during those stages are reviewed in greater detail.

A. Exponential growth and magnetic trapping of the beam particles

During the extensively studied[3–6,9,16,19] early stage of the WI, the electron beam of initial density $n_{b0} < n_0$ and radius $R_{\text{init}} \gg c/\omega_{pe}$ breaks up into a large number of filaments with a typical radius $R \sim c/2\omega_{p0}$. During the linear stage of the instability, magnetic field energy grows exponentially with the growth rate of order Γ_{WI}. This stage comes to an abrupt end when beam electrons inside the filament become trapped and start executing betatron oscillations with the frequency $\Omega_B \sim \Gamma_{\text{WI}}$ and amplitude of order c/ω_{p0}. Results of a representative simulation with $n_{b0}/n_0 = 0.01$ shown in Fig. 4 demonstrate the trapping effect and its correlation with the saturation of the exponential growth of the WI. According to Fig. 4(a), exponential growth stops at around $\omega_{p0}t \approx 270$. This moment corresponds to the onset of particle trapping. In Fig. 4(b), two representative beam particles A and B start executing large-amplitude betatron oscillations with $\Omega_B \approx 0.9\Gamma_{\text{WI}}$ approximately at the same time. The two particles belong to two distinct beam filaments shown in Fig. 4(c). At the trapping onset $n_b/n_0 \approx 0.1$, so the beam filaments have been density compressed by an order of magnitude. Further growth of the magnetic energy proceeds through filaments merger.

B. Expulsion of the ambient plasma from current filaments

Although the QN of the beam-plasma system given by Eq. (2) is preserved during the nonlinear stage of filaments' merger and compression, the beam electron density increases until the background plasma electrons are expelled from the filament: $n_b \approx n_0$. The formation of EPV filaments can be clearly seen in full-PIC simulations. Initially small EPV fila-

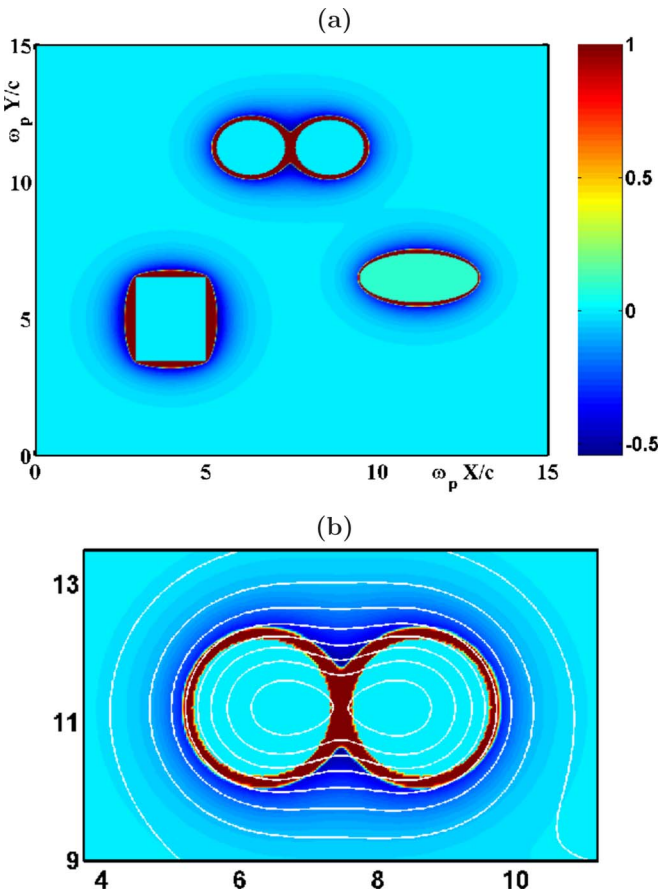

FIG. 3. (Color online) Calculation of the plasma response to externally injected beams with $v_{b0}=0.95c$ in the framework of the QE code. (a) Normalized charge density $\delta N=(n_0-n_e-n_b)/n_0$ for four uniformly charged electron beams: two round and one square-shaped beams with $n_b=n_0$, and one ellipse-shaped beam with $n_b=0.9n_0$. (b) Zoom-in in the vicinity of the two round beams. Color: δN; contours: ψ=const (magnetic field lines). Note the regions of complete electron plasma expulsion.

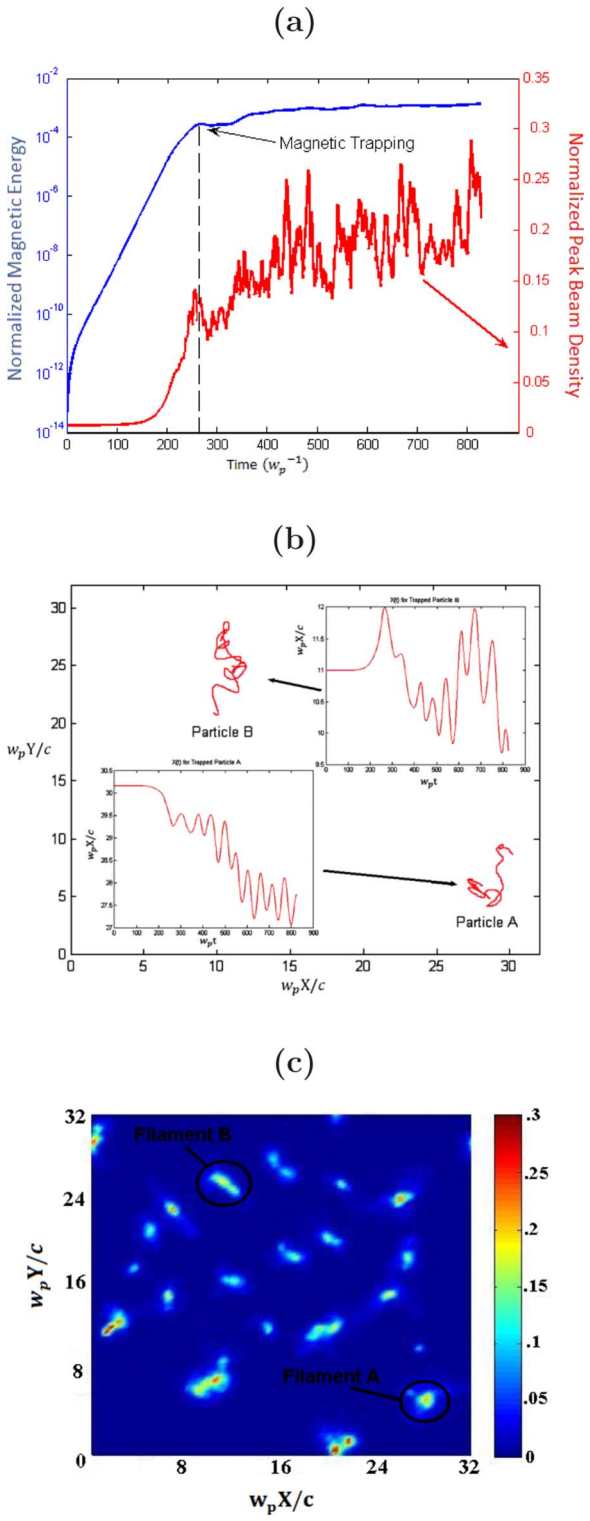

FIG. 4. (Color online) (a) Time evolution of the magnetic energy (normalized to the beam energy) and peak beam density (normalized to ion density) inside the filaments. (b) Magnetic trapping of two representative beam particles A and B trapped in two separate filaments. (c) Electron beam density distribution n_b/n_0 at $t=600\omega_p^{-1}$ and the two filament trapping particles A and B.

ments continue merging, with the corresponding growth of the magnetic field energy. Eventually, their radius R exceeds c/ω_{p0}. Density and current profiles of such filament with $R=5c/\omega_{p0}$ from the simulation with the same parameters as in Fig. 1 are shown in Fig. 5. Note the complete expulsion of the electron plasma from the filament, and a well-defined edge of the electron beam density. Both direct current of the beam and the return current of the ambient plasma are concentrated at the edge of the filament, as explained below. Note that such current and density structure (flat density, localized at the periphery current) is strongly reminiscent of the Hammer–Rostoker[22,31] equilibria of charge-neutralized self-pinched electron beams carrying $I \gg I_A$. Remarkably, magnetic energy density that initially grows due to the merger of the small current filaments gives way to magnetic energy decay as the filaments get larger. Theoretical explanation of this phenomenon[23] is sketched below.

C. Structure and merger of multi-I_A current filaments

In analyzing the merger of two beam/plasma filaments with the initial beam radii R_0 and currents I_0 into a single filament of beam radius $R_1=\sqrt{2}R_0$ (which follows from conservation of particles for the cylindrical beams with $n_b=n_0$) and current I_1, we pose here and answer below the following question: What is the change in the magnetic energy $\Delta U_B \equiv U_{B1}-2U_{B0}$ and filament current $\Delta I \equiv I_1-2I_0$ as the result of the merger?

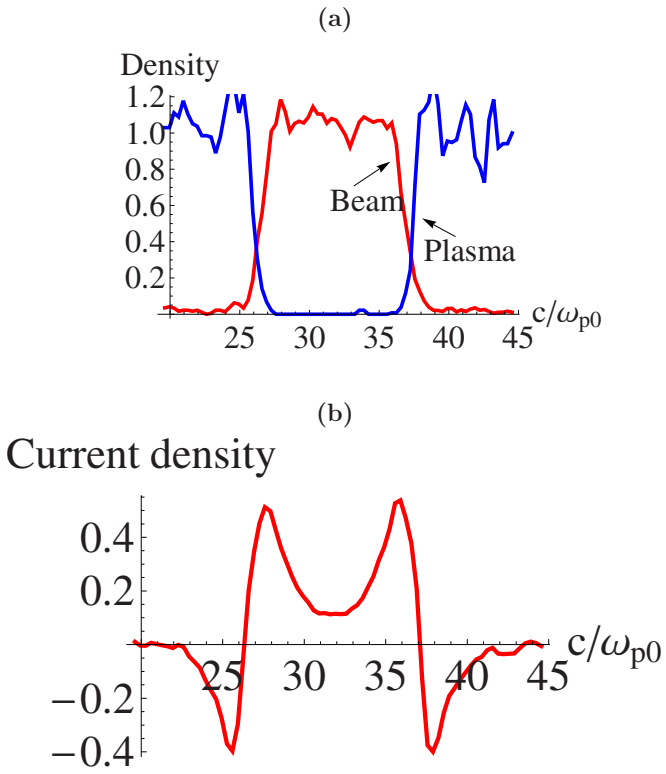

FIG. 5. (Color online) Cross section of an EPV filament at $t=1300\omega_{p0}^{-1}$ carrying the total current $I=4I_A$ shown in Fig. 1(d). (a) Normalized beam and plasma densities n_b/n_0 (beam) and n_p/n_0 (plasma). Note a fairly accurate charge neutrality of the filament. (b) Normalized current density $-j/en_0c$.

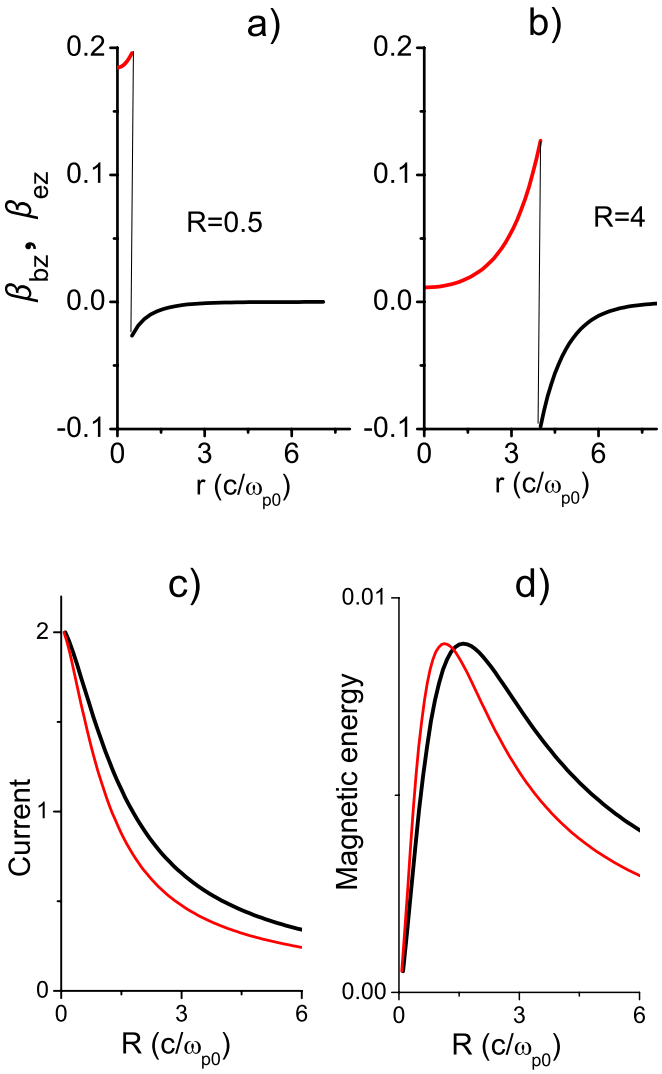

FIG. 6. (Color online) Theory: merger of two nonrelativistic filaments with the initial (prefilamentation) $\beta_{bz0}=0.2$. Top panel: beam and plasma velocity profiles for (a) small ($R=0.5c/\omega_{p0}$) and (b) large ($R=4c/\omega_{p0}$) individual filaments before the merger. Bottom panel: (c) current and (d) energy content of the two filaments of initial radius R before the merger (black curves) and after the merger (red/gray curves).

We start by estimating the magnetic energy of a single evacuated cylindrical beam filament with the beam density $n_b=n_0$ for $r<R$ and $n_b=0$ for $r>R$. The beam filament is surrounded by the return current of the ambient plasma with density $n_e=n_0$ for $r>R$ and $n_e=0$ for $r<R$. We assume that the initial electron beam with the forward momentum $\vec{P}=\vec{e}_z p_{b0}$ is underdense with respect to the quiescent ambient plasma: $n_{b0}\lesssim n_0$. The following normalized quantities are used below: $\tilde{x}=\omega_{pe}x/c$, $\tilde{t}=\omega_{p0}t$, $\tilde{n}=n/n_0$, $\beta_{e,bz}=v_{e,bz}/c$, and $\tilde{p}_{e,bz}=p_{e,bz}/mc$. Tildes are dropped in what follows. Using conservation of the longitudinal canonical momentum, fluid momentum of the beam in the filament is given by $p_{bz}(r)=p_{b0}+\psi(r)$. Substituting $p_{bz}(r)$ into Eq. (4) and using the nonrelativistic expression for v_{pz}, we obtain $\nabla_\perp^2\psi-\psi=\theta(r)\beta_{b0}$, where $\theta(r<R)=1$ and $\theta(r>R)=0$.

The resulting equation was solved to obtain the profiles of the beam's and plasma's axial velocities shown in Figs. 6(a) and 6(b) for a thin ($R=0.5$) and thick ($R=4$) filaments. The beam velocity is strongly peaked at the filament's periphery whenever $R\gg 1$. An electron beam filament with $R\gg 1$ carries a super-Alfvenic current: $I_b/I_A^0=R^2I_1(R)K_1(R)/2$. For $R\gg 1$ this expression is simplified to $I_b/I_A^0\approx R/4>1$, while for $R\ll 1$ we find that $I_b/I_A^0\approx R^2/4\ll 1$.

Note that the beam and plasma velocities as well as the filaments' beam current and the magnetic energy are parametrized by only two parameters: the initial beam velocity β_{b0} and the filament's radius R. These quantities are calculated for two noninteracting filaments of radius R_0 before merger and one resulting (coalesced) filament with radius $R_1=\sqrt{2}R_0$. Normalized beam current and magnetic field energy are expressed as $\bar{I}_b(R)=2\int_0^R drr\beta_{bz}/\beta_{b0}R^2$ and $\bar{U}_B(R)=\int_0^\infty drr|\partial_r\psi|^2/R^2$. The initial (premerger) current and energy are given, respectively, by $2\bar{I}_b(R_0)$ and $2\bar{U}_B(R_0)$. The same postmerger quantities are given by $\bar{I}_b(R_1)$ and $\bar{U}_B(R_1)$. Both premerger (black curves) and postmerger (red curves) quantities are plotted in Figs. 6(c) and 6(d). Independent of the filaments' radius R_0, the total current of the merged filament is decreased during the merger. Remarkably, the total magnetic energy can either increase (for $R<R_{crit}\approx 1.3$) or decrease (for $R>R_{crit}$) as the result of the merger, as shown in Fig. 6(d).

Qualitatively, the merger of two small sub-Alfvenic beam filaments results in the addition of the single filament currents: $\bar{I}_b(R_1)\approx 2\bar{I}_b(R_0)$. This is because for $R<1$, the filament's current is distributed across the entire filament, as

shown in Fig. 6(a), and is therefore approximately proportional to its area. Correspondingly, the total magnetic field energy approximately doubles as the result of the merger. In case of wide super-Alfvenic filaments, the beam current is concentrated within the skin depth c/ω_{pe} of its periphery, as shown in Fig. 6(b). The peripheral region of large filament decreases by a factor $\sim\sqrt{2}$ compared to two smaller filaments before merger. Therefore, the total current of the merged filaments decreases by a factor $\sim\sqrt{2}$ and consequently the total magnetic field energy decreases approximately by the same factor during the merger.

The case of the relativistic electron beam is more complicated because plasma electrons also become relativistic, and because of the formation of the ion sheath surrounding the electron beam. This effect has been neglected by earlier[23] calculations. Note that the nonrelativistic calculation did not rely on any assumptions about the transverse motion of the beam particles: just the conservation of the longitudinal canonical momenta was sufficient for determining the beam and plasma currents. This is no longer the case when relativistic filaments coalesce. For analytic tractability, we consider the merger of two identical magnetically self-confined filaments with the beam particles in HR equilibrium:[22,31] $f_{\rm ini}\propto\delta(\gamma-\gamma_{\rm ini})\delta(\bar{p}-p_{b0})$ and $f_{\rm fin}\propto\delta(\gamma-\gamma_{\rm fin})\delta(\bar{p}-p_{b0})$. Here $\gamma_{\rm ini}$ and $\gamma_{\rm fin}$ are the premerger and postmerger beam energies, $\bar{p}\equiv\gamma_j\beta_{jz}-\psi(\vec{x})$ is the conserved canonical momentum, and δ is the Dirac delta function.

Ambient plasma electrons forming the return current are treated as a cold relativistic fluid with $\beta_{ez}=\psi/\sqrt{1+\psi^2}$. Equation (4) is solved in conjunction with Eq. (9) for the electron density n_e. Additional constraint is imposed: Beam particles turn around at the beam edge: $\gamma^2=1+[p_{b0}+\psi(R)]^2$. This enables relating γ to the beam radius R and the initial (prefilamentation) beam momentum p_{b0}. Therefore, as in the nonrelativistic case, both the beam filaments' current and magnetic field are determined by just two parameters: the beam radius R and the beam initial (prefilamentation) relativistic momentum p_{b0}. Numerically obtained solutions for the plasma and velocities are presented in Figs. 7(a) and 7(b) for narrow ($R=0.5$, $\gamma_{\rm ini}=3.08$) and wide ($R=4$, $\gamma_{ini}=2.18$) filaments with $\beta_{b0}=0.95$. Note a narrow ion sheath at the edge of the electron beam. This sheath is a direct consequence of our assumption of the HR (monoenergetic) distribution of the beam particles that corresponds to the hard density edge. For finite energy spread of the beam electrons, the fully void of the electron plasma ion sheath is likely to disappear.

Just as in the nonrelativistic case, we consider the energetics of the coalescence of two relativistic filaments with the radii R_0 and relativistic energy per particle $\gamma_0 mc^2$ into a single relativistic filament with radius $R_1=\sqrt{2}R_0$ and per particle energy $\gamma_1 mc^2$. The previously defined normalized beam current $\bar{I}_b(R)$ and magnetic energy $\bar{U}_B(R)$ are plotted in Figs. 7(c) and 7(d) for two isolated filaments with R_0 (black line) and a single merged filament with R_1 (red line). As in the nonrelativistic case, coalescence of small filaments leads to the magnetic energy increase, while the merger of large filaments ($R>R_{\rm crit}\approx 3$) reduces the magnetic energy. As Fig.

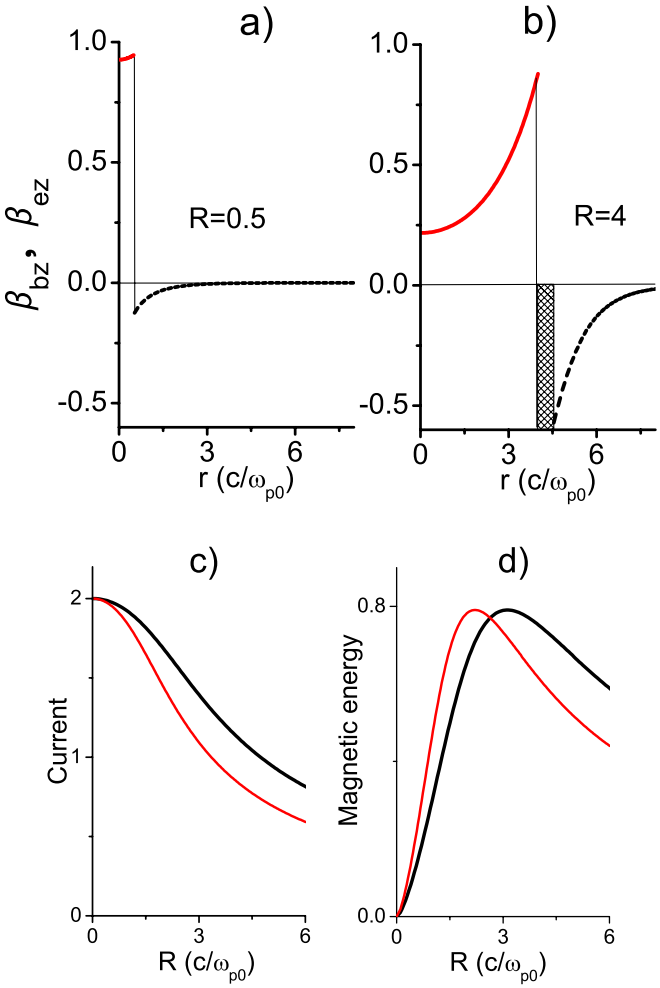

FIG. 7. (Color online) Theory: merger of two relativistic filaments with the initial (prefilamentation) $\beta_{bz0}=0.95$. Top panel: beam and plasma velocity profiles for (a) small ($R=0.5c/\omega_{p0}$) and (b) large ($R=4c/\omega_{p0}$) individual filaments before the merger. Shaded region in (b): non-neutral ion sheath void of beam and plasma electrons. Bottom panel: (c) current and (d) energy content of the two filaments of initial radius R before the merger (black curves) and after the merger (red/gray curves).

1(a) clearly indicates, merger of large filaments results in the energy transfer from the magnetic field to the plasma. In that respect, the late stages of the WI are reminiscent of the magnetic reconnection which is also characterized by the energy transfer from magnetic fields to the plasma. Figure 1(a) reveals abrupt ("stepwise") changes in the beam current and energy, as well as that of the energy of the magnetic field, corresponding to the merger of large current filaments.

IV. EFFECTS OF THE MOVING IONS

In Secs. II and III an important assumption of infinitely heavy (fixed) ions has been made. Ion motion can significantly alter the long-term dynamics of the WI. We have carried out full-PIC (LSP) simulations with the same parameters as in Fig. 1, but with moving ions. A snapshot of the electron beam and ion densities is shown in Fig. 8 for $t=250/\omega_{p0}$. Qualitatively, just as in the fixed-ion case, an electron beam breaks up into EPV filaments that merge and increase/decrease magnetic field energy depending on their size. One

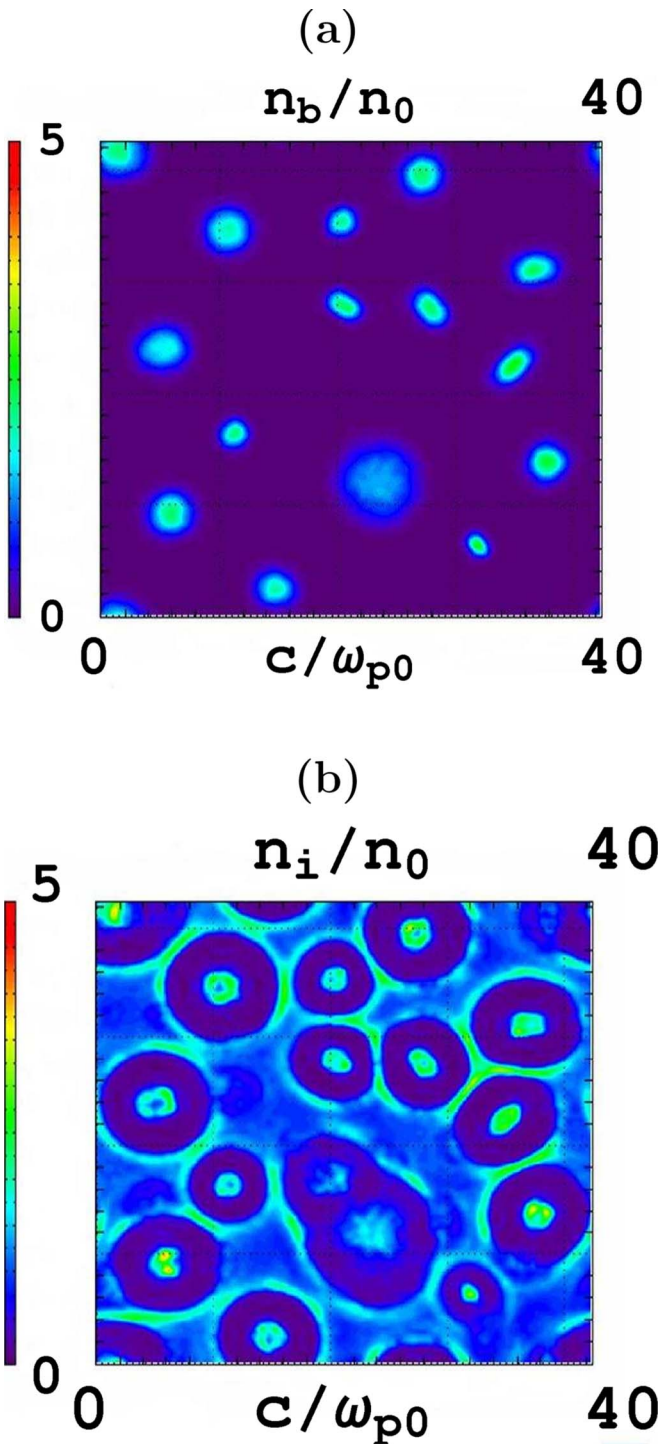

FIG. 8. (Color online) WI with moving ions. Top: concentration of beam electrons (normalized to the initial ion density n_0). Bottom: ion concentration normalized to their initial concentration.

important difference from the fixed-ion case is that with the ion density no longer fixed, electron beam filaments can be compressed to higher densities. Figure 8 indicates that both n_b and n_i can reach $n_b=n_i\approx 3n_0$ densities. Moreover, as the adjacent filaments merger, some of the ions are expelled out of the filaments and compressed between them to similarly high densities. We speculate that longer simulations will reveal a mechanism of ion acceleration reminiscent of the Fermi acceleration due to the ion collisions with multiple filaments. Despite the highly compressed densities of both electrons and ions, we have found that charge neutrality is preserved with high accuracy everywhere except in the narrow sheaths surrounding the EPV regions.

V. CONCLUSIONS

In conclusion, we have reviewed our recent theoretical work on the 2D WI of relativistic electron beams in the plasma. Several novel modeling techniques (QN and QE simulations) have been introduced. We have emphasized the nonlinear long-term behavior of the WI and described several nonlinear phenomena: magnetic particle trapping, development of EPV filaments, and merger between small and large EPV filaments. A simple semianalytical model describing the energetics of merging between two relativistic super-Alfvenic EPV filaments has been developed. Our model predicts, and PIC simulations confirm, that such mergers are responsible for the magnetic energy decay during the late stages of the WI.

ACKNOWLEDGMENTS

This work was partially supported by the U.S. DOE Grant Nos. DE-FG02-05ER54840 and DE-FG02-04ER41321. Carl Siemon gratefully acknowledges the support by the Department of Energy Computational Science Graduate Fellowship. We thank E. Startsev, U. Keshet, A. Pukhov, A. Sefkow, and S. Kalmykov for fruitful discussions.

[1] E. W. Weibel, Phys. Rev. Lett. **2**, 83 (1959).
[2] B. D. Fried, Phys. Fluids **2**, 337 (1959).
[3] R. L. Morse and C. W. Nielson, Phys. Fluids **14**, 830 (1971).
[4] R. C. Davidson, D. A. Hammer, I. Haber, and C. E. Wagner, Phys. Fluids **15**, 317 (1972).
[5] R. Lee and M. Lampe, Phys. Rev. Lett. **31**, 1390 (1973).
[6] M. V. Medvedev and A. Loeb, Astrophys. J. **526**, 697 (1999).
[7] M. V. Medvedev, M. Fiore, R. A. Fonseca, L. O. Silva, and W. B. Mori, Astrophys. J. Lett. **618**, L75 (2005).
[8] A. Gruzinov, Astrophys. J. Lett. **563**, L15 (2001).
[9] L. O. Silva, R. A. Fonseca, J. W. Tonge, W. B. Mori, and J. M. Dawson, Phys. Plasmas **9**, 2458 (2002).
[10] M. Milosavljevic, E. Nakar, and A. Spitkovsky, Astrophys. J. **637**, 765 (2006).
[11] A. Spitkovsky, Astrophys. J. Lett. **673**, L39 (2008).
[12] M. Tabak, J. Hammer, M. E. Glinsky, W. L. Kruer, S. C. Wilks, J. Woodworth, E. M. Campbell, M. D. Perry, and R. J. Mason, Phys. Plasmas **1**, 1626 (1994).
[13] J. J. Honrubia and J. Meyer-ter-Vehn, Nucl. Fusion **46**, L25 (2006).
[14] S. Atzeni and J. Meyer-ter-Vehn, *The Physics of Inertial Fusion* (Oxford University Press, New York, 2004), p. 409.
[15] T. Taguchi, T. M. Antonsen, C. S. Liu, and K. Mima, Phys. Rev. Lett. **86**, 5055 (2001).
[16] R. A. Fonseca, L. O. Silva, J. W. Tonge, W. B. Mori, and J. M. Dawson, Phys. Plasmas **10**, 1979 (2003).
[17] V. M. Malkin and N. J. Fisch, Phys. Rev. Lett. **89**, 125004 (2002).
[18] J. M. Hill, M. H. Key, S. P. Hatchett, and R. R. Freeman, Phys. Plasmas **12**, 082304 (2005).
[19] O. Polomarov, A. Sefkow, I. Kaganovich, and G. Shvets, Phys. Plasmas **14**, 043103 (2007).
[20] M. Honda, J. Meyer-ter-Vehn, and A. Pukhov, Phys. Rev. Lett. **85**, 2128 (2000).
[21] L. O. Silva, R. A. Fonseca, J. W. Tonge, J. M. Dawson, W. B. Mori, and M. Medvedev, Astrophys. J. Lett. **596**, L121 (2003).

[22]R. C. Davidson, *Physics of Nonneutral Plasmas* (Addison-Wesley, Reading, MA, 1990), p. 122.
[23]O. Polomarov, I. Kaganovich, and G. Shvets, Phys. Rev. Lett. **101**, 175001 (2008).
[24]Ya. B. Fainberg, V. D. Shapiro, and V. I. Shevchenko, Sov. Phys. JETP **30**, 528 (1970) [Zh. Eksp. Teor. Fiz. **57**, 966 (1969)].
[25]M. Lampe and P. Sprangle, Phys. Fluids **18**, 475 (1975).
[26]M. E. Dieckmann, B. Eliasson, P. K. Shukla, N. J. Sircombe, and R. O. Dendy, Plasma Phys. Controlled Fusion **48**, B303 (2006).
[27]A. Bret, M.-C. Firpo, and C. Deutsch, Phys. Rev. Lett. **94**, 115002 (2005).
[28]B. I. Cohen, A. B. Langdon, D. W. Hewett, and R. J. Procassini, J. Comput. Phys. **81**, 151 (1989).
[29]LSP is a software product of ATK Mission Research, Albuquerque, NM 87110.
[30]T. N. Kato, Phys. Plasmas **12**, 080705 (2005).
[31]D. A. Hammer and N. Rostoker, Phys. Fluids **13**, 1831 (1970).
[32]E. P. Lee, S. Yu, H. L. Buchanan, F. W. Chanbers, and M. N. Rosenbluth, Phys. Fluids **23**, 2095 (1980).
[33]I. D. Kaganovich, G. Shvets, E. Startsev, and R. C. Davidson, Phys. Plasmas **8**, 4180 (2001).
[34]O. Buneman, Proc. R. Soc. London, Ser. A **215**, 346 (1952).